J Solid State Electrochem (2017) 21:243–253
DOI 10.1007/s10008-016-3367-4

ORIGINAL PAPER

Impedimetric evaluation of hybrid cationic porphyrin/quantum dot multilayer assemblies: a biocompatible interface for calf thymus DNA immobilization

Camilo García[1] · **Freddy Navarro**[1] · **Domingo Ruíz-León**[2] · **Olimpo García Beltrán**[3] · **María Jesús Aguirre**[1]

Received: 16 March 2016 / Revised: 3 August 2016 / Accepted: 12 August 2016 / Published online: 24 August 2016

Abstract In this work, a cationic porphyrin, ascribed as $[Ttolyl(P\text{-}(C_6H_5)_3)_4]^{4+}$, where Ttolyl = 5,10,15,20 tetrakistolylporphyrin, was electrostatically assembled with CdTe quantum dots capped with glutathione (GSH) of diameter ~3.28 nm via a layer-by-layer methodology. This multilayer assembly was evaluated as a biocompatible interface with synergic effects for calf thymus double-stranded DNA (CT DNA) immobilization, considering that the hybrid assembly contains a cationic porphyrin with a high binding constant for CT DNA, and quantum dots with polypeptide as a capping agent. The multilayer assembly, ascribed as ITO/$\{[Ttolyl(P\text{-}(C_6H_5)_3)_4]^{4+}$/CdTe$\}_n$ (n = 1–5), was characterized by UV-Vis spectroscopy, cyclic voltammetry, and electrochemical impedance spectroscopy (EIS). The last technique was explored in order to check the adsorption of CT DNA onto the multilayer porphyrin/quantum dot assembly. The difference in electron transfer resistance (ΔR_{ct}) obtained after CT DNA incubations showed the best result for a specific multilayer assembly, n = 3. $\{[Ttolyl(P\text{-}(C_6H_5)_3)_4]^{4+}$/CdTe$\}_3$ showed a good correlation of ΔR_{ct} with the logarithmic concentration of CT DNA, in the range 1.0×10^{-10} to 1.0×10^{-6} M with a limit of detection (LOD) of 1.5×10^{-12} M. Conversely, when the $\{[Ttolyl(P\text{-}(C_6H_5)_3)_4]^{4+}$/CdTe$\}_3$ system was incubated with calf thymus single-stranded DNA and salmon testes DNA, no significant difference in ΔR_{ct} was observed. We conclude that the newly described $\{[Ttolyl(P\text{-}(C_6H_5)_3)_4]^{4+}$/CdTe$\}_n$ system is a choice method for the impedimetric determination of CT DNA.

Keywords Cationic porphyrins · Quantum dots · DNA-porphyrin interactions · Layer by layer assemblies · Calf thymus DNA determination

Electronic supplementary material The online version of this article (doi:10.1007/s10008-016-3367-4) contains supplementary material, which is available to authorized users.

✉ Camilo García
camilo.garcia.s@usach.cl

[1] Facultad de Química y Biología, Departamento de Química de los Materiales, Laboratorio de Polímeros Conductores, Universidad de Santiago de Chile, Avenida Libertador Bernardo O'Higgins, 3363 Estación Central, Chile

[2] Facultad de Química y Biología, Departamento de Química de los Materiales, Laboratorio de Electroquímica del Estado Sólido, Universidad de Santiago de Chile, Avenida Libertador Bernardo O'Higgins, 3363 Estación Central, Chile

[3] Facultad de Ciencias Naturales y Matemáticas, Universidad de Ibagué, Carrera 22 Calle 67, Ibagué 730001, Colombia

Introduction

Layer-by-layer techniques are extensively employed to modify surfaces because the material quantity, electronic properties, and thickness of the films generated can be easily controlled [1]. Moreover, these modified surfaces can be used as biosensors and bioelectronic devices, because synergetic effects between the components of the multilayer arrangements improve the biocompatibility of the electrodic interface [2]. Furthermore, the study of new systems that interact with DNA biomolecules is interesting from the perspective of designing new bioelectrochemical interfaces [3–6].

Tetra-(triphenyl)-phosphoniumtolylporphyrin has been demonstrated to have electrostatic interactions with genomic calf thymus double-stranded DNA (CT DNA) in solution, at difference of other cationic porphyrins that intercalate between aromatic domains and grooves of DNA [7–9]. Alternately, CdTe quantum dots are semiconductor nanomaterials based on the II/IV family [10] with emission

properties tunable by their size and with biocompatibility easily modulated by employing amino acids or polypeptides, such as cysteine or glutathione [11, 12].

Hybrid cationic porphyrins/CdTe quantum dots electrostatically assembled have been studied in solution by photophysical techniques [13], and their analytical applications were recently demonstrated in the detection of CT DNA, generated by hybrids acting as on-off fluorescent sensors [14–16].

To our knowledge, there are not examples of the properties of such hybrids assembled onto electrodic surfaces in CT DNA detection.

There are two main types of research concerning DNA detection. One of them requires DNA immobilization onto electrodic surface for using it for DNA sequencing, detecting DNA damage or for hybridization biosensors [6, 17]. This methodology can be used in the diagnosis of infectious diseases, genetic mutations, clinical medicine, and forensic applications [18–20]. On the other hand, the direct detection of native or double-stranded DNA, where immobilization is incompatible, is of interest for industrial biopharmaceutical laboratories where sensitive, simple, and rapid methods for DNA determination in solution are required [21].

DNA immobilization based on electrochemical techniques has been proposed as an alternative to conventional DNA detection techniques, because electrochemical techniques are cheaper, transportable, and easily miniaturized [17, 22–25].

Some groups have focused its efforts on CT DNA determination based on the increasing of the oxidation current of guanine by voltammetric techniques employing carbon paste or glassy carbon electrodes modified with nanomaterials as transducers [6, 26, 27]. Another way, in this work we present evidence on the feasibility of a hybrid system of porphyrins/quantum dots that presents a different behavior measured by electrochemical impedance spectroscopy (EIS) when CT DNA immobilization takes place. For that purpose, we use a common redox couple such as $[Fe(CN)_6]^{3-}/[Fe(CN)_6]^{4-}$ to detect and differentiate CT DNA immobilization. This approach is an alternative procedure to voltammetric analysis, when voltammetric peaks observed for CT DNA detection are poorly defined.

From the broad spectra of electrochemical techniques, EIS has gained attention as a label-free DNA hybridization transduction [4, 5, 28] because phosphate groups of single-stranded or double-stranded DNA species can be easily discriminated in the presence of anionic redox species, such as $[Fe(CN)_6]^{3-}/[Fe(CN)_6]^{4-}$ [17].

This work describes the characterization of hybrids $\{[Ttolyl(P\text{-}(C_6H_5)_3)_4]^{4+}/CdTe\}_n$ by UV-Vis spectroscopy, SEM microscopy, cyclic voltammetry, and EIS, and their analytical performance in CT DNA determination by EIS. We provide evidence supporting the use of the $\{[Ttolyl(P\text{-}(C_6H_5)_3)_4]^{4+}/CdTe\}_n$ system for the detection and quantification of CT DNA.

Materials and methods

Apparatus

UV-Vis spectroscopy was performed with a Scinco S-3100 spectrometer. Emission spectra were recorded with a Luminescence spectrometer Perkin Elmer LS 50 B irradiating at 350 nm in a quartz cuvette with an optical pass of 1.0 cm.

^{1}H-NMR characterization was performed in a Bruker 400. Cyclic voltammetry and EIS were registered in a CH-Instrument 604C. Data from the impedance measurements were obtained by fitting with Z view® software. A one-compartment cell was employed with three electrodes, where indium tin oxide (ITO), Delta Technologies, with a resistance of 20–30 Ω and a geometric area of 1.5 cm^2 was employed as a working electrode, Ag/AgCl (3 M KCl) was used as a reference electrode, and a platinum coil was used as an auxiliary electrode. Electrochemical impedance spectroscopy was measured between 100 kHz and 10 MHz with the application of E_{DC} = +0.2 V. The sinusoidal potential pulse was 5 mV.

Scanning electron microscopy with energy dispersive X-ray spectroscopy (SEM-EDX) analyses were obtained from a high-resolution imaging via a Vegan 3 Tescan microscope coupled to a Bruker Quantax 400 energy dispersive X-ray detector.

Reagents

Diisobutylaluminium hydride (DIBAL-H) was acquired from Alfa Aesar Company. Bromotolylbenzonitrile, triphenylphosphine, cloroanile, boron trifluorideetherate, triethylamine, single-stranded deoxyribonucleic acid genomic from calf thymus (CT ssDNA), deoxyribonucleic acid genomic, type XV from calf thymus (CT DNA), deoxyribonucleic acid genomic from salmon testes (ST DNA), and Tween 20® were purchased from Sigma-Aldrich. The concentration of the starting standard was determined by its absorbance at 260 nm, assuming $\varepsilon = 10{,}560\ M^{-1}\ cm^{-1}$ for CT ssDNA, $\varepsilon = 13{,}100\ M^{-1}\ cm^{-1}$ [8] for CT DNA, and $\varepsilon = 12{,}824\ M^{-1}\ cm^{-1}$ for ST DNA [29].

Tris-(hydroxymethyl)-aminomethane and *N*-(2-hydroxyethyl)-ethylenediamine-*N*,*N*′,*N*′-triacetic acid (EDTA; molecular biology grade, Calbiochem), methanol, toluene, and n-hexane were obtained from Merck. Pyrrole was acquired from Sigma-Aldrich, and it was distilled prior to use. DIBAL-H was manipulated by avoiding contact with air and water.

Synthesis

5,10,15,20-tetra(triphenylphosphonium)tolylporphyrin was synthesized via a procedure described elsewhere [7]. Yield

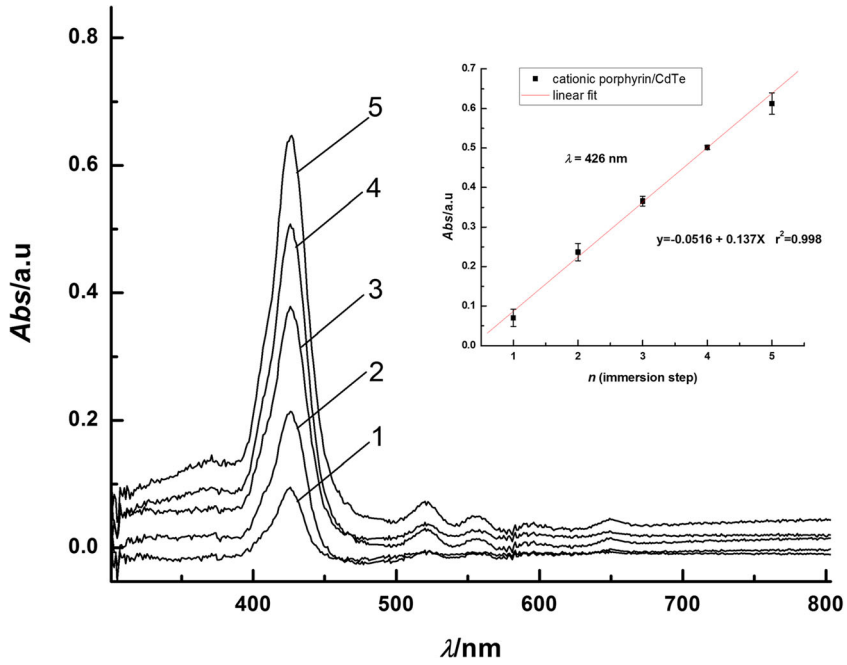

Fig. 1 UV-Vis spectra of the layer-by-layer assemblies of ITO/$\{[Ttolyl(P\text{-}(C_6H_5)_3)_4]^{4+}/CdTe\}_n$, where n is the number of immersion steps, with a range from 1 to 5. *Inset*: absorbance at 426 nm vs n

(32 %), ^{1}H-NMR ($CD_3Cl + CD_3OD$): 8.76 (s, 8H, β-pyrrole), 8.05 (d, 8H, phenyl-CH_2), 7.83–7.89 (m, 60H, P-phenyl), 7.46 (m, 8H, phenyl-CH_2). FT-IR/cm^{-1} (in KBr): 3394, 3034 (m, =NH), 2859 (m, C–H on phenyl and pyrroles), 1618 (m, C = N imines), 1438 (C = C), 1111 (s, CH_2-P). UV-Vis (CH_3OH) 416 nm, log ε/M^{-1} cm^{-1} = 5.7 ($\pi - \pi^*$ transition Soret band), 514, 548, 591, 644 ($\pi - \pi^*$ transition, Q bands). CdTe (GSH) was synthesized according to a procedure described elsewhere [11, 30]. λ_{em} = 582 nm (orange emission). The diameter size was estimated as ~3.28 nm by UV-Vis spectroscopy.

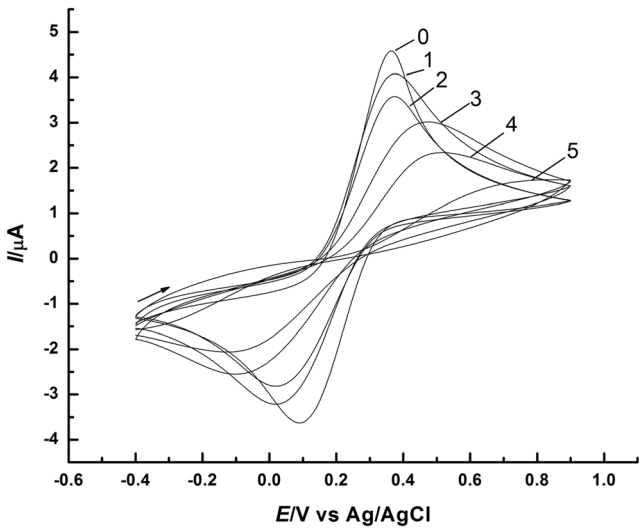

Fig. 2 Cyclic voltammetry of layer-by-layer assemblies of ITO/$\{[Ttolyl(P\text{-}(C_6H_5)_3)_4]^{4+}/CdTe\}_n$, where n is the immersion step, with n ranging from 1 to 5, in the presence of 2.0 mM $Fe(CN)_6^{4-}/Fe(CN)_6^{3-}$, 10 mM Tris, and 0.1 M KCl

ITO pretreatment

ITO electrodes were activated by refluxing them at 105 °C in a solution consisting of NH_4OH, H_2O_2, and H_2O in a 1:1:5 proportion for 1.0 h, and the solution was agitated at 250 rpm. They were washed gently with bi-distilled water and then dried under a nitrogen stream.

Layer-by-layer electrostatic self-assemblies

ITO electrodes were immersed inside a solution of 0.1 mM tetra tolyl(triphenyl)phosphoniumporphyrin in a 10 mM Tris buffer, at a pH of 7.0 and with 8 % methanol, for 5 min. After the porphyrin layer deposition, the electrodes were washed with abundant water and dried with an N_2 stream. After this, the electrodes were immersed inside a solution of CdTe (GSH) quantum dot in a 10 mM Tris buffer at a pH of 10 for 5 min. Then the electrode was cleaned with abundant deionized water and dried with an N_2 stream. The process was repeated to obtain a higher number of multilayers. Every step was monitored by UV-Vis spectroscopy, cyclic voltammetry, and electrochemical impedance spectra in the presence of 2.0 mM $[Fe(CN)_6]^{3-}/[Fe(CN)_6]^{4-}$ in 10 mM Tris at a pH of 7.0 and 0.1 M KCl.

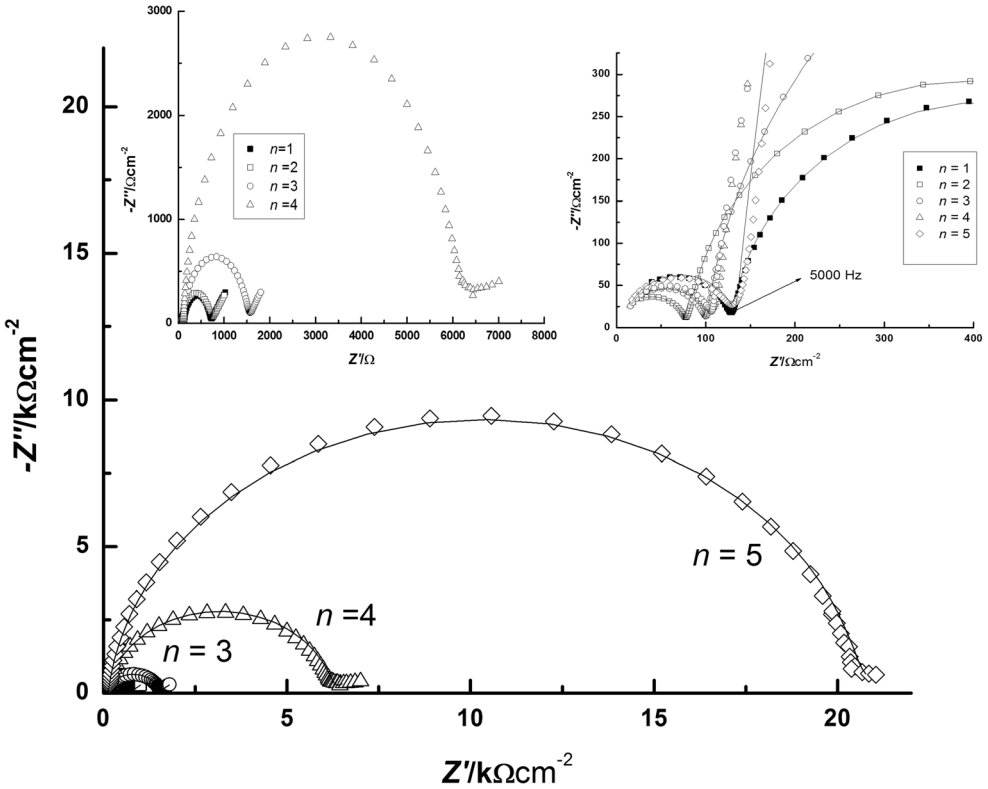

Fig. 3 Nyquist plots from electrochemical impedance spectra of different bi-layers onto ITO surfaces. Two millimolar $Fe(CN)_6^{4-}/Fe(CN)_6^{3-}$, 10 mM Tris, and 0.1 M KCl. Potential of +0.2 V applied vs Ag/AgCl. Amplitude pulse potential = 5 mV. Frequency range = 0.01 Hz–100 kHz

Native DNA adsorption onto $\{[Ttolyl(P\text{-}(C_6H_5)_3)_4]^{4+}/CdTe\}_n$

ITO electrodes modified with $\{[Ttolyl(P\text{-}(C_6H_5)_3)_4]^{4+}/CdTe\}_n$ with n = 1, 3, and 5 were incubated for 30 min in solutions of CT DNA (calf thymus), ST dsDNA (salmon testes), or CT ssDNA (calf thymus) at 60 °C. After every incubation step, each electrode was gently washed with an aqueous solution of 0.05 % Tween® 20 and bi-distilled water and then dried with an N_2 stream in order to eliminate any weakly adsorbed DNA molecules.

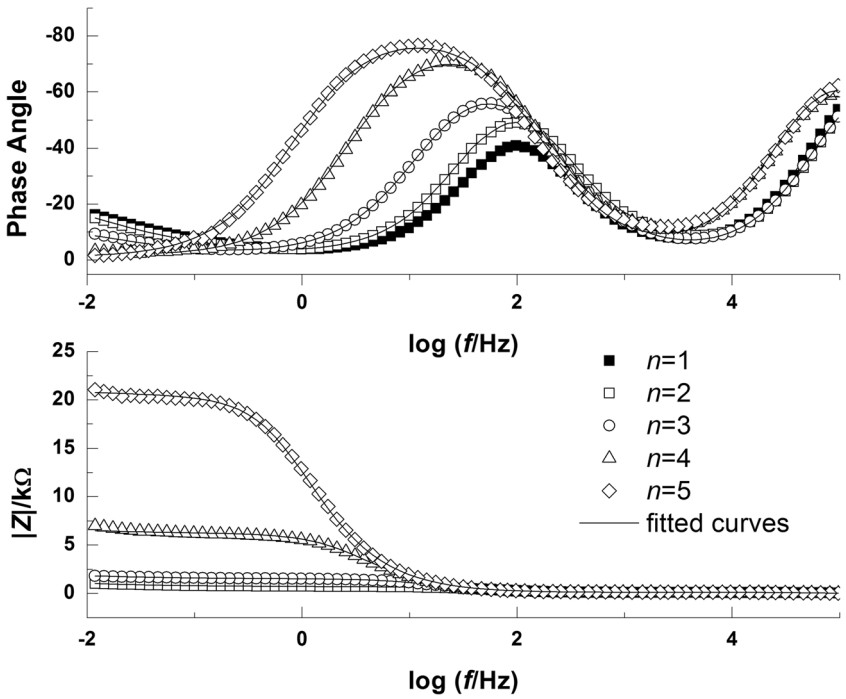

Fig. 4 Bode plots of different layer-by-layer onto ITO surfaces. Two millimolar $Fe(CN)_6^{4-}/Fe(CN)_6^{3-}$, 10 mM Tris, and 0.1 M KCl. Potential of +0.2 V applied vs Ag/AgCl. Amplitude pulse potential = 5 mV. Frequency range = 0.01 Hz–100 kHz

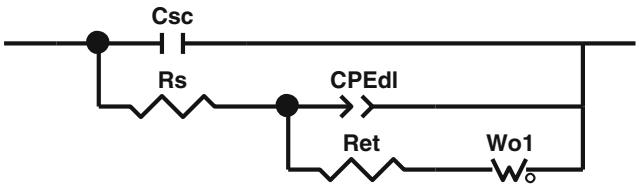

Scheme 1 Equivalent circuit employed. *Csc* ITO semiconductor capacitance, R_s solution resistance, CPE_{dl} constant phase element for electric double layer, R_{et} resistance to electron transfer, W_{o1} Warburg diffusional impedance

Results and discussion

Characterization of the $\{[Ttolyl(P\text{-}(C_6H_5)_3)_4]^{4+}/CdTe\}_n$ assemblies

UV-Vis spectroscopy

Figure 1 shows the UV-Vis spectra of the $\{[Ttolyl(P\text{-}(C_6H_5)_3)_4]^{4+}/CdTe\}_n$ hybrid. In all multilayer assemblies, the most intense peak appears at 426 nm and is associated with a $\pi - \pi^*$ electronic transition of cationic porphyrins, known as Soret band [30–32]. The absorbance of such band for these systems increased linearly with every new immersion step *n*, providing evidence that the porphyrins are being adsorbed in a layer-by-layer approach with the corresponding quantum dots [33–35]. The inset of Fig. 1 shows the Soret band for triplicate experiments, with a linear response related to the immersion steps, showing the accuracy of the methodology. It must be denoted that these spectra are slightly different to a previous work, where a smaller size of CdTe quantum dots was employed [30]. In the current work, only electronic transitions associated with porphyrins are present, and there is not exciton absorption of CdTe quantum dots ($d = 3.28$ nm) in the multilayer assembly.

Cyclic voltammetry of $\{[Ttolyl(P\text{-}(C_6H_5)_3)_4]^{4+}/CdTe\}_n$ assemblies

Figure 2 shows the behavior of the ITO/$\{[Ttolyl(P\text{-}(C_6H_5)_3)_4]^{4+}/CdTe\}_n$ in 2.0 mM $Fe(CN)_6^{4-}/Fe(CN)_6^{3-}$, where it can be observed clearly the presence of pinhole across the multilayer [30, 36]. The $Fe(CN)_6^{4-}/Fe(CN)_6^{3-}$ couple presented a quasi-reversible behavior in the presence of the ITO electrode ($n = 0$), with a peak potential difference ΔE_p of +0.27 V. However, in the presence of ITO/$\{[Ttolyl(P\text{-}(C_6H_5)_3)_4]^{4+}/CdTe\}_{1–3}$ multilayer assemblies, $Fe(CN)_6^{4-}/Fe(CN)_6^{3-}$ couple presented a higher ΔE_p compared to that of the ITO electrode, corresponding to +0.36, +0.35, and +0.37 V, respectively. The current value diminished for every immersion step, demonstrating that the surface is changing when the multilayer assembly is formed. A more irreversible behavior of the probe $Fe(CN)_6^{4-/}Fe(CN)_6^{3-}$ in the presence of ITO/$\{[Ttolyl(P\text{-}(C_6H_5)_3)_4]^{4+}/CdTe\}_{4–5}$ was observed because its ΔE_p was +0.60 V when $n = 4$, whereas the current associated with the $Fe(CN)_6^{4-}/Fe(CN)_6^{3-}$ couple yielded a plateau shape at $n = 5$. These results can be associated with a sluggish electron transfer for every new immersion step performed for ITO/$\{[Ttolyl(P\text{-}(C_6H_5)_3)_4]^{4+}/CdTe\}_n$ systems in the presence of the $[Fe(CN)_6]^{3-}/[Fe(CN)_6]^{4-}$ redox couple. The decrease in the current for the $[Fe(CN)_6]^{3-}/[Fe(CN)_6]^{4-}$ probe and the more irreversible character of the peak potentials from $n = 3$ to $n = 5$ are due to the electrostatic repulsion between the anionic CdTe in the multilayer assembly and the $[Fe(CN)_6]^{3-}/[Fe(CN)_6]^{4-}$, which can be attributed to the increasing electrostatic repulsion and the increasing covering of the surface. A similar behavior was previously reported for other electrostatic multilayer assemblies [30, 36].

This electrostatic effect can be confirmed when similar characterization is performed in the presence of a cationic redox probe, such as $[Ru(NH)_5Cl]^{2+}$ (see Figure S1), where it was observed that ΔE_p slightly changes for every new immersion step from 0.16 V ($n = 1$) to 0.19 V ($n = 5$). The current value slightly decreases for every new immersion step. A similar behavior has been published previously for other electrostatic multilayer assemblies. The electroactive area for each ITO/$\{[Ttolyl(P\text{-}(C_6H_5)_3)_4]^{4+}/CdTe\}_n$ system showed slight variations compared to the electroactive area of the ITO electrode, providing evidence that electrostatic repulsions are playing an important role, more so than the disposable nanometer area with CdTe capped with glutathione.

Table 1 Electrochemical impedance data obtained by fitting ITO/$\{[Ttolyl(P\text{-}(C_6H_5)_3)_4]^{4+}/CdTe$ (3.28 nm)$\}_n$, where $n = 1–5$, in the presence of 2 mM $Fe(CN)_6^{4-}/Fe(CN)_6^{3-}$, 10 mM Tris, and 0.1 M KCl. Potential of +0.2 V applied vs Ag/AgCl; amplitude pulse potential = 5 mV; frequency range = 0.01 Hz–100 kHz

	$R_s/\Omega cm^{-2}$	$CPE\text{-}T/\mu Ccm^{-2}$	*CPE-P*	$R_{et}/\Omega cm^{-2}$	$\tau\,(C_{dl}R_{et})$/ms	ω/s^{-1}	C_{ITO}/nF
0	113.3	10.6	0.945	592.5	4.67	34.0	4.8
1	127.9	9.13	0.941	577.0	3.79	42.0	22.8
2	78.2	11.2	0.937	626.5	5.03	31.7	29.5
3	99.9	12.2	0.927	1415	12.5	12.7	23.7
4	100.9	11.3	0.941	6039	57.8	2.76	58.9
5	130.3	10.5	0.942	20,402	194.6	0.82	42.3

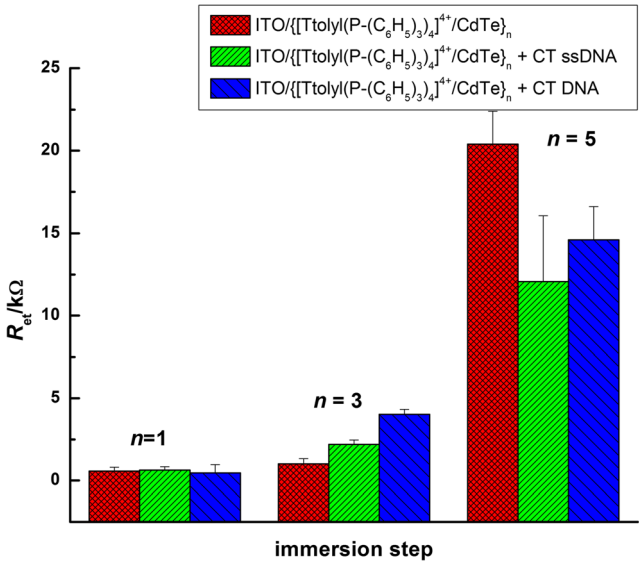

Fig. 5 Resistance to charge transfer of ITO/{[Ttolyl(P-$(C_6H_5)_3)_4$]$^{4+}$/CdTe}$_{1,3,5}$ after incubation in 1.0×10^{-6} M CT DNA obtained by EIS in the presence of 2 mM $Fe(CN)_6^{4-}/Fe(CN)_6^{3-}$, 10 mM Tris, and 0.1 M KCl. E_{dc} = +0.2 V vs Ag/AgCl. Sinusoidal potential = 5 mV. Frequency range = 0.01 Hz–100 kHz

Electrochemical impedance spectroscopy

Figure 3 shows the characteristic Nyquist plot obtained when the ITO electrode was immersed in an alternating manner in porphyrin and CdTe quantum dot solutions. An incomplete semicircle region (100 kHz to ~5000 Hz) associated with the inner capacitance of semiconductors was observed at higher frequencies [37, 38]. At frequencies lower than 5000 Hz, the electrochemical interfacial process can be observed, where the semicircle region can be associated with the resistance to the electron transfer between the $[Fe(CN)_6]^{3-}/[Fe(CN)_6]^{4-}$ redox couple and a linear region associated with the mass transfer processes, the Warburg impedance.

Figure 4 shows Bode plots for every immersion step. It was observed that at high frequencies, the phase angle starts at ~−45°, in the semiconductor zone, but all spectra show a peak process associated with the time constant of the $[Fe(CN)_6]^{3-}/[Fe(CN)_6]^{4-}$ redox couple in the electrochemical interface. The module of impedance clearly shows the predominance of two resistances, a $|Z|$ constant one associated with the solution resistance R_s at frequencies lower than 5000 Hz, and the resistance to electron transfer at frequencies lower than 1 Hz, where the $|Z|$ module reaches a plateau, associated with the resistance to the electron transfer of $[Fe(CN)_6]^{3-}/[Fe(CN)_6]^{4-}$. The presence of a double-layer capacitor was evident because the $|Z|$ changes with frequency. Taking all of this information into consideration, the proposed equivalent circuit is displayed in Scheme 1. This circuit generates two time constants, as it can be observed in angle phase vs frequency plot, and demonstrates their combination zone of semiconductor and the electrochemical interface where the electrochemical reaction is occurring [38]. The χ-square of all the fits is lower than 0.002, confirming the good accuracy of the equivalent circuitry proposed. A constant phase element (CPE), instead of an ideal capacitor for double-layer capacitance, was employed because this type of impedance element is useful when the interface is not flat, such as the multilayer assemblies studied in this work. $Z_{CPE} = 1/(T_{(i\omega)})^P$, where the value of the P exponent changes from 0 to 1. Depending on this value, T can take resistance (~0) or capacitance (~1) units, showing the more resistive or capacitive behavior of the system [39]. Table 1 provides the values for the circuitry elements proposed. The predominant parameter that changes for every new immersion step is R_{ct}. When $n = 0$ and $n = 1$, R_{ct} exhibited a similar value; however, from $n = 2$ to $n = 5$, R_{ct} increases for every new immersion step, demonstrating the electrostatic repulsion between $[Fe(CN)_6]^{3-}/[Fe(CN)_6]^{4-}$ and the anionic outer layer CdTe in these

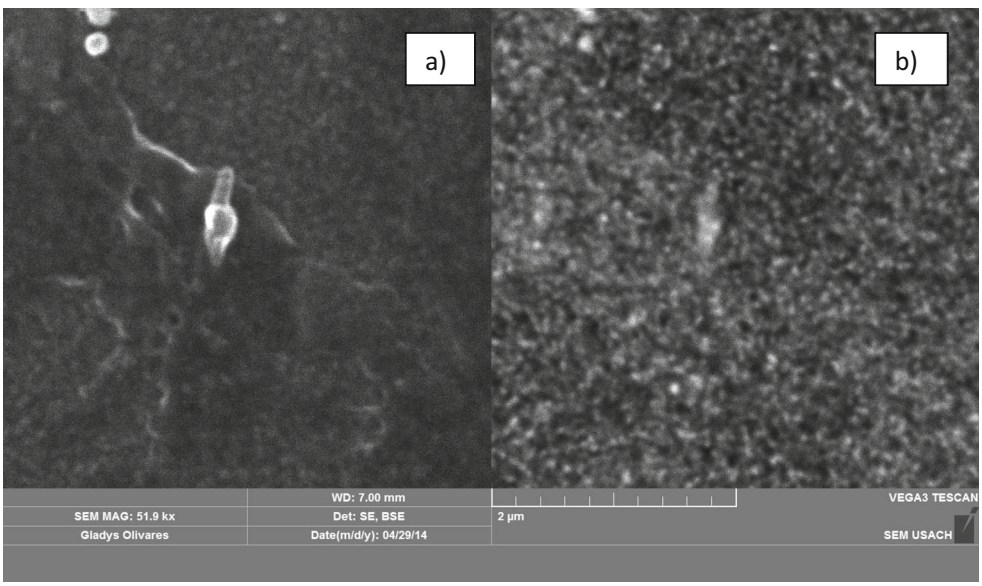

Fig. 6 SEM microscopy of ITO/{[Ttolyl(P-$(C_6H_5)_3)_4$]$^{4+}$/CdTe}$_3$ after adsorption of CT DNA 1.0×10^{-6} M. **a** Mode. **b** Backscattering electrons

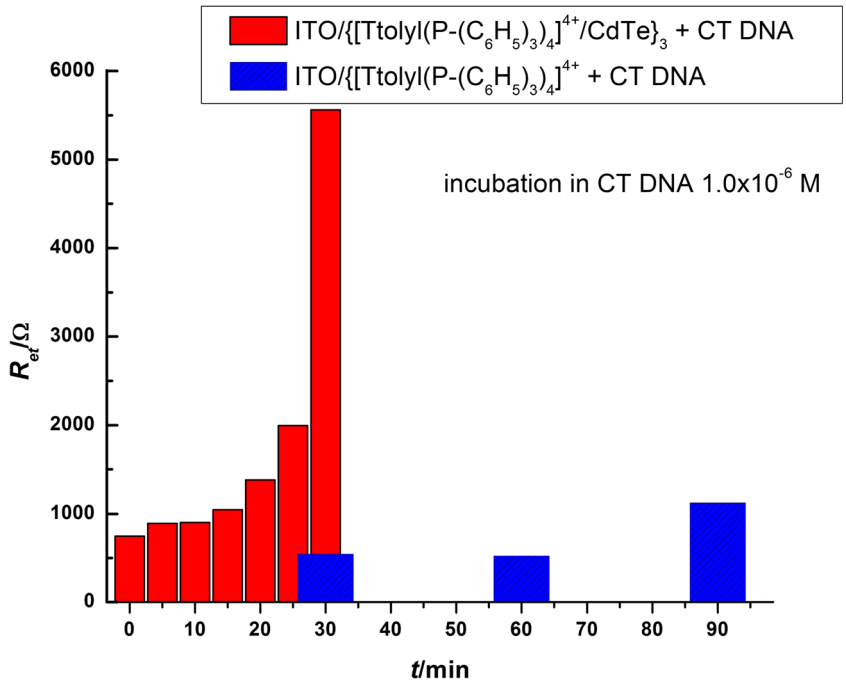

Fig. 7 Time optimization with ITO/{[Ttolyl(P-$(C_6H_5)_3)_4]^{4+}$/CdTe}$_3$ and ITO/[Ttolyl(P-$(C_6H_5)_3)_4]^{4+}$ after incubation in 1.0×10^{-6} M CT DNA obtained by EIS in the presence of 2.0 mM $Fe(CN)_6^{4-}/Fe(CN)_6^{3-}$, 10 mM Tris, and 0.1 M KCl. Potential of +0.2 V applied vs Ag/AgCl. Sinusoidal pulse potential = 5 mV. Frequency range = 0.01 Hz–10 kHz

assemblies. In a similar pattern, the relaxation time ($\tau = C_{dl}R_{ct}$) for every multilayer increased in the range of 3.79 to 174.6 ms, showing a more sluggish process for $[Fe(CN)_6]^{3-}/[Fe(CN)_6]^{4-}$ by increasing n. Inversely, the characteristic frequency for ITO/{[Ttolyl(P-$(C_6H_5)_3)_4]^{4+}$/CdTe}$_n$ in the presence of $[Fe(CN)_6]^{3-}/[Fe(CN)_6]^{4-}$ diminishes with n in the range 42.0 to 0.82 s^{-1}.

To corroborate the electrostatic effect of these assemblies, $Ru(NH_3)_5^{3+}$ was used as the redox couple for ITO/{[Ttolyl(P-$(C_6H_5)_3)_4]^{4+}$/CdTe}$_n$. The ITO electrode shows a diffusional pattern only with a phase angle close to −45° against this redox couple. However, when ITO/{[Ttolyl(P-$(C_6H_5)_3)_4]^{4+}$/CdTe}$_n$ systems were immersed in the solution containing cationic ruthenium species, a semicircle was observed in the Nyquist plots, associated with the presence of the multilayer assemblies. Nonetheless, the diameter of the semicircle is almost constant between n = 1–4. Only when n = 5 there was an increase compared to the early step of modification (see Figure S2). The electron transfer resistance after fitting the spectra with a typical Randles circuitry shows a low dependence on the immersion step, suggesting that the predominantly anionic character of outer layer helps the external sphere electron to the transfer of $Ru(NH_3)_5^{3+}$ toward the ITO electrode. This pattern was observed in other electrostatic multilayer assemblies studied by EIS [21, 36].

Finally, the capacitance of the semiconductor zone changed significantly compared to the control with ITO, and it is three orders of magnitude order lower than the capacitance obtained from C_{dl}.

Interactions of {[Ttolyl(P-$(C_6H_5)_3)_4]^{4+}$/CdTe}$_n$ with genomic DNA

Assuming that the equivalent circuitry in Scheme 1 is valid, it was proposed to study the absorption of DNA species by {[Ttolyl(P-$(C_6H_5)_3)_4]^{4+}$/CdTe}$_n$ considering R_{ct}, taking into consideration its strong influence on DNA species as was explained above.

Optimization of the multilayer number

Figure 5 shows the R_{ct} obtained from EIS of {[Ttolyl(P-$(C_6H_5)_3)_4]^{4+}$/CdTe}$_n$, where n = 1, 3, and 5, before and after incubation of these hybrids in 1.0×10^{-6} M of CT DNA and CT ssDNA, in separate experiments. No significant changes in R_{ct} of the multilayer assembly were observed with n = 1 and n = 5. However, the R_{ct} of the system {[Ttolyl(P-$(C_6H_5)_3)_4]^{4+}$/CdTe}$_3$ could differentiate CT ssDNA or CT DNA, demonstrating its ability to be immobilized even if the outer layer is negative CdTe quantum dots. The difference is probably associated with the repulsion of $[Fe(CN)_6]^{3-}/[Fe(CN)_6]^{4-}$ redox couple with the different number phosphate groups in single- and double-stranded DNA. It can be seen from the results that the multilayer hybrid has a specific immersion step that is able to differentiate CT DNA, with n = 3 being the optimum multilayer number.

SEM-EDX microscopy of ITO/{[Ttolyl(P-$(C_6H_5)_3)_4]^{+}$/CdTe}$_3$ after CT DNA incubation

The morphology of the ITO/{[Ttolyl(P-$(C_6H_5)_3)_4]^{+}$/CdTe}$_3$ system is very similar to that of our previous work [30].

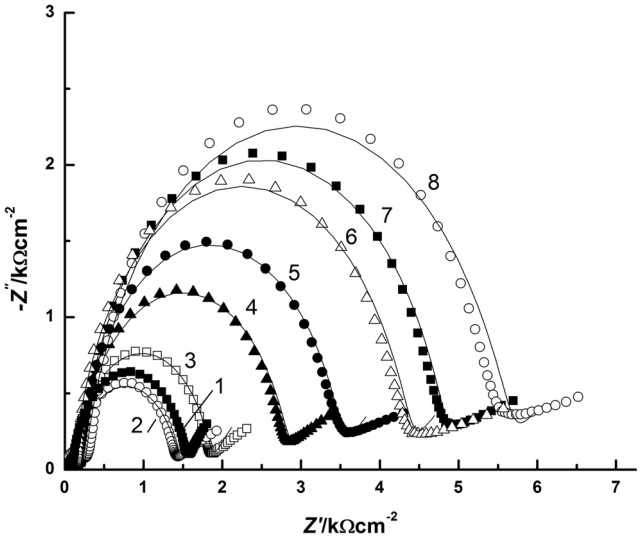

Fig. 8 Nyquist plot of ITO/{[Ttolyl(P-$(C_6H_5)_3)_4$]$^{4+}$/CdTe}$_3$ after incubation at different concentrations of genomic DNA: *curve 1* (0 DNA); *2* (CT ssDNA 0.6 × 10^{-6} M); *3* (1.0 × 10^{-6} M ST DNA); *4–8* CT DNA at concentrations: *4* (1.0 × 10^{-10} M); *5* (1.0 × 10^{-9} M); *6* (1.0 × 10^{-8} M); *7* (1.0 × 10^{-7} M); and *8* (1.0 × 10^{-6} M)

However, here, we propose that CT DNA was effectively adsorbed onto the ITO/{[Ttolyl(P-$(C_6H_5)_3)_4$]$^{+}$/CdTe}$_3$, as can be observed in Fig. 6a. An organic layer is adsorbed onto the ITO electrode providing evidence for the presence of cationic porphyrin and CT DNA. However, as it is observed from backscattered electrons (see Fig. 6b), a homogeneous surface of spherical-like particles spreads over the ITO electrode. The quantum dots are agglomerated on the electrode surface, showing a mean size of 80 nm, which is larger than those obtained from UV-Vis measurements in solution [30]. The morphology pattern suggests that CT DNA was immobilized onto ITO/{[Ttolyl(P-$(C_6H_5)_3)_4$]$^{+}$/CdTe}$_3$.

Effect of CdTe (GSH) on CT DNA adsorption

To corroborate the effect of CdTe quantum dots on CT DNA immobilization, R_{ct} was evaluated after different incubation times in 1.0 × 10^{-6} M CT DNA between a layer of porphyrin ascribed as ITO/{[Ttolyl(P-$(C_6H_5)_3)_4$]$^{4+}$ and the hybrid ITO/{[Ttolyl(P-$(C_6H_5)_3)_4$]$^{4+}$/CdTe}$_3$ (Fig. 7). It was observed that after incubation in the CT DNA solution, ITO/{[Ttolyl(P-$(C_6H_5)_3)_4$]$^{4+}$/CdTe}$_3$ required 20 to 30 min to change the R_{ct}, whereas ITO/{[Ttolyl(P-$(C_6H_5)_3)_4$]$^{4+}$ required 90 min to change; hence, CdTe nanoparticles help in the rapid immobilization of 1.0 × 10^{-6} M CT DNA on ITO/{[Ttolyl(P-$(C_6H_5)_3)_4$]$^{4+}$/CdTe}$_3$.

As the outer layer of ITO/{[Ttolyl(P-$(C_6H_5)_3)_4$]$^{4+}$/CdTe}$_3$ consists of negatively charged quantum dots, other non-covalent forces could be influencing the adsorption of CT DNA onto the multilayer assembly, as corroborated by the SEM micrograph. To this respect, it was recently reported that CdTe capped with glyphosate can immobilize CT DNA by non-covalent interactions, such as hydrogen bonding and DNA [40].

At this point, it is clear that a synergic effect between cationic porphyrin/CdTe immobilized onto ITO is helping in the adsorption of CT DNA. This effect on the multilayer assembly was corroborated by UV-Vis spectroscopy, because the Soret band of porphyrin diminishes its absorbance after immobilization of 1.0 × 10^{-6} M CT DNA (see Figure S3), as it could be expected from its behavior in solution with CT DNA [7–9].

Analytical performance of ITO/{[Ttolyl(P-$(C_6H_5)_3)_4$]$^{+}$/CdTe}$_3$

EIS is a valuable tool for studying the adsorption processes of DNA onto electrodic surfaces because negative charged redox couples can be repealed by the electrostatic action of phosphate groups present in the DNA backbone [17]. As it can be

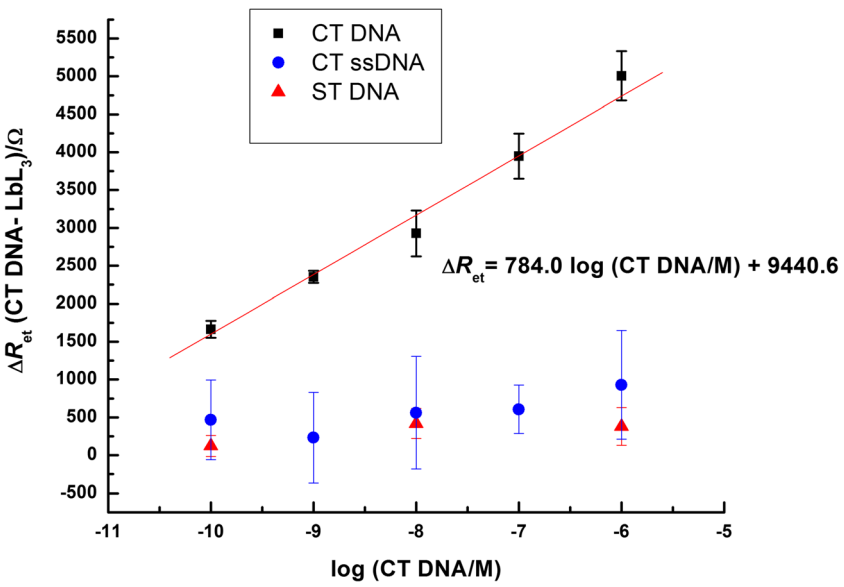

Fig. 9 R_{ct} of ITO/{[Ttolyl(P-$(C_6H_5)_3)_4$]$^{4+}$/CdTe}$_3$ by triplicate experiments in the presence of 2.0 mM $Fe(CN)_6^{4-}$/$Fe(CN)_6^{3-}$ obtained by EIS after genomic DNA incubations. Ten millimolar Tris, pH = 7.0, and 0.1 M KCl. Potential of +0.2 V applied vs Ag/AgCl. Amplitude sinusoidal pulse = 5 mV. Frequency range = 0.01 Hz–100 kHz

Table 2 Comparison of the analytical parameters for CT DNA determination

Work	Range linearity	LOD	Technique
[14]	6.5×10^{-9}–29.6×10^{-8} M	2.72×10^{-9} M	Fluorescence
[40]	0.109–70 μg/mL	0.0327 μg/mL	Fluorescence
[21]	1.0×10^{-7}–1.0×10^{-4} g/mL	9.6×10^{-8} g/mL	EIS
[6]	5–60 μg/mL	0.971 μg/mL	DPV
This work	1.0×10^{-10}–1.0×10^{-6} M	6.0×10^{-11} M	EIS
	(1.3×10^{-8}–1.3×10^{-5} g/mL)	7.8×10^{-10} g/mL	

observed in Fig. 8, after CT DNA incubations, there was a significant increase in R_{ct} at higher CT DNA concentrations. In contrast, after incubation in CT ssDNA and ST DNA, the R_{ct} of ITO/$\{[Ttolyl(P\text{-}(C_6H_5)_3)_4]^+/CdTe\}_3$ varied slightly, from 1415 to1724 Ω and from 1415 to 1315 Ω, respectively. These results show that CT DNA is being expediently adsorbed onto ITO/$\{[Ttolyl(P\text{-}(C_6H_5)_3)_4]^+/CdTe\}_3$, whereas the CT ssDNA and ST DNA species are being poorly adsorbed.

Figure 9 shows a representative R_{ct} signal response as a function of the concentration of CT DNA. R_{ct} increases linearly with the logarithm of CT DNA, as can be expected for an affinity experiment when a broad range of concentrations are studied, such as in this work [41]. No correlations with the concentrations of the corresponding CT ssDNA and ST DNA were observed in the range of concentrations studied. These results suggest that ITO/$\{[Ttolyl(P\text{-}(C_6H_5)_3)_4]^+/CdTe\}_3$ can specifically bind to CT DNA instead of other typical genomic DNA species. The reproducibility of the present method was excellent: the standard deviation for four replications at a concentration of 1.0×10^{-8} M was 7.68 %.

The impedimetric sensor for CT DNA was compared with other sensors for this biomolecule. As observed in Table 2, the proposed sensor has a broader concentration range, and a lower LOD compared to other reports [6, 14, 21, 41], making the proposed ITO/$\{[Ttolyl(P\text{-}(C_6H_5)_3)_4]^+/CdTe\}_3$ hybrid system a good candidate for the determination of genomic CT DNA.

Finally, cyclic voltammetry after DNA incubations showed an irreversible oxidation associated with the typical guanine oxidation at +1.2 V (see Figure S4). The signal associated with this process was broad and poor defined at low CT DNA concentration, and it is not present after CT ssDNA incubation, validating the idea of the utilization of EIS to study the CT DNA adsorption onto the ITO/$\{[Ttolyl(P\text{-}(C_6H_5)_3)_4]^+/CdTe\}_3$ system.

Conclusion

Hybrid $\{[Ttolyl(P\text{-}(C_6H_5)_3)_4]^{4+}/CdTe\}_n$ specimens, where $n = 1$–5, were prepared by immersion steps, and they were characterized by UV-Vis spectroscopy, cyclic voltammetry, and EIS.

The immersion steps of the hybrid system and the time to immobilize DNA species were optimized by EIS. It was found that ITO/$\{[Ttolyl(P\text{-}(C_6H_5)_3)_4]^+/CdTe\}_3$ has synergic effects on the immobilization of CT DNA by electrochemical impedance spectroscopy, cyclic voltammetry, and UV-Vis spectroscopy. ITO/$\{[Ttolyl(P\text{-}(C_6H_5)_3)_4]^+/CdTe\}_3$ was demonstrated as selectively adsorbing CT DNA instead of other genomic species with a linear range of 1.0×10^{-10} to 1.0×10^{-6} M and a LOD of 6.0×10^{-11} M using EIS. SEM-EDX microscopy of ITO/$\{[Ttolyl(P\text{-}(C_6H_5)_3)_4]^+/CdTe\}_3$ after incubation in CT DNA showed a film on the CdTe capped with glutathione, and backscattering microscopy confirmed that CdTe was spread over all of the surface. These results suggest that CT DNA could be specifically immobilized by both electrostatic attraction (cationic porphyrin) and hydrogen bonds CdTe (GSH).

This work is a first approach for the use of hybrid cationic porphyrin/quantum dot assemblies to adsorb biomolecules onto electrodic surfaces; this interface brings about multiple binding sites to CT DNA via non-covalent interactions. Overall, the results indicate that the newly described $\{[Ttolyl(P\text{-}(C_6H_5)_3)_4]^{4+}/CdTe\}_n$ system is an excellent method for the determination of CT DNA.

Acknowledgments Camilo García thanks the FONDECYT program regarding Initiation FONDECYT grant 11150434 and Postdoctoral Project 3130328. M. J Aguirre expresses thanks regarding FONDECYT grant 1160324.

References

1. Shen Y, Zhan F, JF L, Zhang BY, Huang DK, XB X, Zhang YB, Wang MK (2013) Preparation of hybrid films containing gold nanoparticles and cobalt porphyrin with flexible electrochemical properties. Thin Solid Films 545:327–331
2. Iost RM, Crespilho FN (2012) Layer-by-layer self-assembly and electrochemistry: applications in biosensing and bioelectronics. Biosens Bioelectron 31(1):1–10
3. Erdem A, Meric B, Kerman K, Dalbasti T, Ozsoz M (1999) Detection of interaction between metal complex indicator and DNA by using electrochemical biosensor. Electroanalysis 11(18): 1372–1376
4. Gupta VK, Yola ML, Qureshi MS, Solak AO, Atar N, Üstündağ Z (2013) A novel impedimetric biosensor based on graphene oxide/gold nanoplatform for detection of DNA arrays. Sensors Actuators B Chem 188:1201–1211
5. Loo AH, Bonanni A, Pumera M (2013) An insight into the hybridization mechanism of hairpin DNA physically immobilized on chemically modified graphenes. Analyst 138(2):467–471

6. Canete-Rosales P, Alvarez-Lueje A, Bollo S (2014) Ethylendiamine-functionalized multi-walled carbon nanotubes prevent cationic dispersant use in the electrochemical detection of dsDNA. Sensors Actuators B Chem 191:688–694
7. Kubat P, Lang K, Anzenbacher P, Jursikova K, Kral V, Ehrenberg B (2000) Interaction of novel cationic meso-tetraphenylporphyrins in the ground and excited states with DNA and nucleotides. J Chem Soc, Perkin Trans 1 6:933–941
8. Kubat P, Lang K, Kral V, Anzenbacher P (2002) Preprogramming of porphyrin-nucleic acid assemblies via variation of the alkyl/aryl substituents of phosphonium tetratolylporphyrins. J Phys Chem B 106(26):6784–6792
9. Kubat P, Lang K, Prochakova K, Anzenbacher P (2003) Self-aggregates of cationic meso-tetratolylporphyrins in aqueous solutions. Langmuir 19(2):422–428
10. Lisdat F, Schafer D, Kapp A (2013) Quantum dots on electrodes—new tools for bioelectroanalysis. Anal Bioanal Chem 405(11): 3739–3752
11. Sheng ZH, Han HY, XF H, Chi C (2010) One-step growth of high luminescence CdTe quantum dots with low cytotoxicity in ambient atmospheric conditions. Dalton Trans 39(30):7017–7020
12. Diaz V, Ramirez-Maureira M, Monras JP, Vargas J, Bravo D, Osorio-Roman IO, Vasquez CC, Perez-Donoso JM (2012) Spectroscopic properties and biocompatibility studies of CdTe quantum dots capped with biological thiols. Sci Adv Mater 4(5–6):609–616
13. Jagadeeswari S, Paramaguru G, Renganathan R (2014) Synthesis and characterization of free base and metal porphyrins and their interaction with CdTe QDs. J Photochem Photobiol A Chem 276: 104–112
14. Vaishnavi E, Renganathan R (2014) "Turn-on-off-on" fluorescence switching of quantum dots-cationic porphyrin nanohybrid: a sensor for DNA. Analyst 139(1):225–234
15. Zhu K, XY H, Ge QY, Sun QJ (2014) Fluorescent recognition of deoxyribonucleic acids by a quantum dot/meso-tetrakis(N-methylpyridinium-4-yl)porphyrin complex based on a photo induced electron-transfer mechanism. Anal Chim Acta 812:199–205
16. Zhao D, Fan Y, Gao F, Yang T-m (2015) "Turn-off-on" fluorescent sensor for (N-methyl-4-pyridyl) porphyrin-DNA and G-quadruplex interactions based on ZnCdSe quantum dots. Anal Chim Acta 888: 131–137
17. Katz E, Willner I (2003) Probing biomolecular interactions at conductive and semiconductive surfaces by impedance spectroscopy: routes to impedimetric immunosensors, DNA-sensors, and enzyme biosensors. Electroanalysis 15(11):913–947
18. Ziolkowski R, Olejniczak AB, Gorski L, Janusik J, Lesnikowski ZJ, Malinowska E (2012) Electrochemical detection of DNA hybridization using metallacarborane unit. Bioelectrochemistry 87: 78–83
19. Wang S, Li L, Jin H, Yang T, Bao W, Huang S, Wang J (2013) Electrochemical detection of hepatitis B and papilloma virus DNAs using SWCNT array coated with gold nanoparticles. Biosens Bioelectron 41:205–210
20. Hu Y, Li F, Han D, Wu T, Zhang Q, Niu L, Bao Y (2012) Simple and label-free electrochemical assay for signal-on DNA hybridization directly at undecorated graphene oxide. Anal Chim Acta 753: 82–89
21. Shervedani RK, Pourbeyram S (2010) Electrochemical determination of calf thymus DNA on Zr(IV) immobilized on gold-mercaptopropionic-acid self-assembled monolayer. Bioelectrochemistry 77(2):100–105
22. Bonanni A, del Valle M (2010) Use of nanomaterials for impedimetric DNA sensors: a review. Anal Chim Acta 678(1):7–17
23. Fojta M, Kostecka P, Trefulka MR, Havran L, Palecek E (2007) "Multicolor" electrochemical labeling of DNA hybridization probes with osmium tetroxide complexes. Anal Chem 79(3): 1022–1029
24. Palecek E, Fojta M (2001) Detecting DNA hybridization and damage. Anal Chem 73(3):74A–83A
25. Spires JB, Peng H, Williams D, Travas-Sejdic J (2011) An improved terthiophene conducting polymer for DNA-sensing. Electrochim Acta 58:134–141
26. Serpi C, Voulgaropoulos A, Girousi S (2013) Electrochemical study of dsDNA on carbon nanotubes paste electrodes applying cyclic and differential pulse voltammetry. Central European Journal of Chemistry 11(3):413–423
27. Thangaraj R, Kumar AS (2013) Simultaneous detection of guanine and adenine in DNA and meat samples using graphitized mesoporous carbon modified electrode. J Solid State Electrochem 17(3): 583–590
28. Yang T, Guo X, Ma Y, Li Q, Zhong L, Jiao K (2013) Electrochemical impedimetric DNA sensing based on multi-walled carbon nanotubes-SnO2-chitosan nanocomposite. Colloids Surf B Biointerfaces 107:257–261
29. Barcelo F, Capo D, Portugal J (2002) Thermodynamic characterization of the multivalent binding of chartreusin to DNA. Nucleic Acids Res 30(20):4567–4573
30. Garcia C, Fuenzalida F, Ruiz D, Jesus Aguirre M (2014) Electrochemical, spectroscopic and morphological characterization of electrostatic self-assembled hybrids of tetracationic phosphonium porphyrins and CdTe quantum dots. J Appl Electrochem 44(12):1345–1353
31. Garcia C, Diaz C, Araya P, Isaacs F, Ferraudi G, Lappin AG, Jesus Aguirre M, Isaacs M (2014) Electrostatic self-assembled multilayers of tetrachromatedmetalloporphyrins/polyoxometalateand its electrocatalytic properties in oxygen reduction. Electrochim Acta 146:819–829
32. Garcia M, Carfuman K, Diaz C, Garrido C, Osorio-Roman I, Aguirre MJ, Isaacs M (2012) Multimetallic porphyrins/polyoxotungstate modified electrodes by layer-by-layer method: electrochemical, spectroscopic and morphological characterization. Electrochim Acta 80:390–398
33. Bazzan G, Smith W, Francesconi LC, Drain CM (2008) Electrostatic self-organization of robust porphyrin-polyoxometalate films. Langmuir 24(7):3244–3249
34. Jin H, Choi S, Velu R, Kim S, Lee HJ (2012) Preparation of multilayered CdSe quantum dot sensitizers by electrostatic layer-by-layer assembly and a series of post-treatments toward efficient quantum dot-sensitized mesoporous TiO2 solar cells. Langmuir 28(12):5417–5426
35. Wang HL, Sun Q, Chen M, Miyake J, Qian DJ (2011) Layer-by-layer assembly and characterization of multilayers of a manganese porphyrin linked poly(4-vinylpyridinium) derivative and poly(styrenesulfonic acid-o-maleic) acid. Langmuir 27(16):9880–9889
36. Fernandes DM, Ghica ME, Cavaleiro AMV, Brett CMA (2011) Electrochemical impedance study of self-assembled layer-by-layer iron-silicotungstate/poly(ethylenimine) modified electrodes. Electrochim Acta 56(23):7940–7945
37. Ozmen M, Maltas E, Patir IH, Bayrakci M (2013) Combined voltammetric and spectroscopic investigation of binding interaction between nifedipine and human serum albumin on polyelectrolyte modified ITO electrode. Electrochim Acta 111:535–542
38. Hens Z, Gomes WP (1999) The electrochemical impedance of one-equivalent electrode processes at dark semiconductor/redox electrodes involving charge transfer through surface states. 2. The n-GaAs/Fe3+ system as an experimental example. J Phys Chem B 103(1):130–138
39. Díaz C, García C, Iturriaga-Vásquez P, Aguirre MJ, Muena JP, Contreras R, Ormazábal-Toledo R, Isaacs M (2013) Experimental and theoretical study on the oxidation mechanism of dopamine in n-

octyl pyridinium based ionic liquids–carbon paste modified electrodes. Electrochim Acta 111(0):846–854

40. Liang WJ, Liu ZQ, Liu SP, Yang JD, He YQ (2014) A novel surface modification strategy of CdTe/CdS QDs and its application for sensitive detection of ct-DNA. Sensors Actuators B Chem 196:336–344

41. Miranda-Castro R, de-los-Santos-Alvarez P, MJ L-C, AJ M-O, Tunon-Blanco P (2007) Hairpin-DNA probe for enzyme-amplified electrochemical detection of Legionella pneumophila. Anal Chem 79(11):4050–4055